mathematics

MDPI

Article

Magnetohydrodynamic Flow and Heat Transfer Induced by a Shrinking Sheet

Nor Ain Azeany Mohd Nasir [1], Anuar Ishak [2,*] and Ioan Pop [3]

[1] Department of Mathematics, Centre for Defence Foundation Studies, Universiti Pertahanan Nasional Malaysia, Kem, Sungai Besi, Kuala Lumpur 57000, Malaysia; norainazeany@upnm.edu.my
[2] Department of Mathematical Sciences, Faculty of Science and Technology, Universiti Kebangsaan Malaysia, UKM Bangi 43600, Selangor, Malaysia
[3] Department of Mathematics, Babes-Bolyai University, 400084 Cluj-Napoca, Romania; ipop@math.ubbcluj.ro
* Correspondence: anuar_mi@ukm.edu.my

Received: 18 June 2020; Accepted: 15 July 2020; Published: 17 July 2020

Abstract: The magnetohydrodynamic (MHD) stagnation point flow over a shrinking or stretching flat sheet is investigated. The governing partial differential equations (PDEs) are reduced into a set of ordinary differential equations (ODEs) by a similarity transformation and are solved numerically with the help of MATLAB software. The numerical results obtained are for different values of the magnetic parameter M, heat generation parameter Q, Prandtl number Pr and reciprocal of magnetic Prandtl number ε. The influences of these parameters on the flow and heat transfer characteristics are investigated and shown in tables and graphs. Two solutions are found for a certain rate of the shrinking strength. The stability of the solutions in the long run is determined, and shows that only one of them is stable. It is found that the skin friction coefficient $f''(0)$ and the local Nusselt number $-\theta'(0)$ decrease as the magnetic parameter M increases. Further, the local Nusselt number increases as the heat generation increases.

Keywords: dual solutions; induced magnetic field; shrinking sheet; stability

1. Introduction

The study of heat and mass transfer in the magnetohydrodynamic (MHD) flow has been considered by many researchers due to its applications in various areas. MHD flow plays important roles in the field of medicine, for example in cancer tumor treatment causing hypothermia, reducing bleeding in severe injuries and magnetic resonance imaging [1]. Famous applications of MHD flows include cooling of nuclear reactors, combustion modelling, geophysics and plasma studies. These applications are affected quantitatively by heat transfer enhancement [2]. The application of MHD flows induced by a magnetic field is widely used in semiconductor industries [3]. An investigation on the MHD viscous fluid flow passing through a moving surface was conducted by Fang et al. [4]. Countless studies have been reported on MHD flows under enormous physical conditions. Such reports can be found in [5,6].

Although there are many studies on MHD flows toward a stretching sheet which can be found in [7,8], there are only a few studies regarding such flows toward a shrinking sheet. For instance, Fang et al. [9] studied the MHD viscous fluid flow over a stretching sheet and reported the exact solution for this problem. They found that the fluid flow and shear stress are greatly affected by partial slip, magnetic parameter and mass transfer. Then Fang and Zhang [10] extended this work to a shrinking sheet and included the injection/suction effect at the boundary. They reported that the velocity decreases as the injection effect is increased, but it increases as the suction strength is increased. The unsteady MHD flow and heat transfer of a nanofluid induced by a shrinking sheet in the presence of thermal radiation were considered by Nandy et al. [11]. They found that the skin

friction coefficient and the Sherwood number increase for the first solution, but decrease for the second solution, for increasing values of the magnetic parameter. Later on, many similar problems were considered and discussed by other authors [12–19].

A stagnation point flow occurs when a flow impinges a solid object [12]. At this point, the velocity of the fluid is zero and has high pressure on the surface of the solid object. The pioneer study of the two-dimensional stagnation point flow was done by Hiemenz [20], who found that the governing Navier–Stokes equations can be reduced to an ordinary differential equation (ODE) using a similarity transformation. Mustafa et al. [21] considered the MHD flow of a ferrofluid towards a stagnation point on a stretchable rotating disk. They solved the problem numerically using the Keller box method. The MHD stagnation point flow of a Maxwell fluid with the effects of an induced magnetic field and convective boundary condition were studied by Ibrahim [22]. The results showed that the skin friction coefficient, the local Sherwood number and the local Nusselt number were inversely proportional to the Maxwell and magnetic parameters. Many investigators have studied the stagnation point flow under different physical situations [23–27].

All of the above-mentioned papers on the MHD flows paid less attention to the effect of the induced magnetic field. Ali et al. [28] investigated the MHD flows with induced magnetic field over a stretching sheet. They also investigated the MHD stagnation point flows with an induced magnetic field over a stretching sheet [29]. The stretching surface is occurring when the velocity at the boundary moves away from a fixed point. This phenomenon can be found in the manufacturing processes such as paper production, plastic sheet extraction and even glass blowing. The stretching surface will usually shrink back. The shrinking surface occurs when the velocity at the boundary moves toward a fixed point. This phenomenon of the shrinking surface is very useful in agriculture. Examples of applications are the study of capillary effects on very small pores, expansion behavior as well as hydraulic properties of clay for agricultural purposes. Hence, different from [28] and [29], in the present paper, we consider both the stretching and shrinking cases. The fluid flow induced by the shrinking sheet is different from that of a stretching sheet. The flow over a shrinking sheet is a kind of backward flow discussed by Goldstein [30].

2. Basic Equations

Consider a magnetohydrodynamic (MHD) flow of a viscous, incompressible and electrically conducting fluid in the stagnation region on a stretching/shrinking surface as shown in Figure 1. The induced magnetic field is taken into consideration in this problem. The stretching/shrinking surface is assumed in the form $\lambda u_w\ (x)$, where λ is the stretching/shrinking parameter with $\lambda > 0$ corresponding to a stretching surface, $\lambda < 0$ corresponds to a shrinking surface and $\lambda = 0$ corresponds to a static surface. Moreover $u_e\ (x) = xa$ is the ambient velocity and $H_e\ (x) = xH_0$ is the ambient magnetic field. Further, the constant temperature of the stretching/shrinking sheet is denoted by T_w, while the ambient fluid temperature is denoted by T_∞.

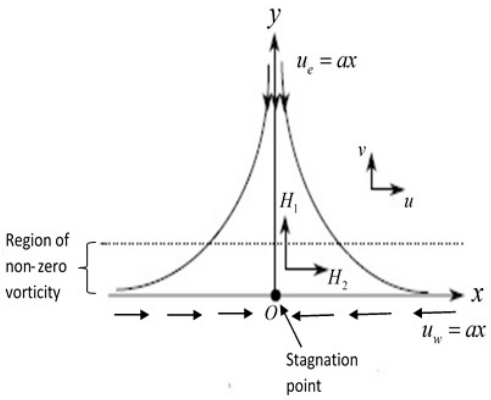

Figure 1. Physical model and coordinate system for the shrinking sheet.

The governing equations are [31]:

$$\frac{\partial u}{\partial x} + \frac{\partial v}{\partial y} = 0, \tag{1}$$

$$\frac{\partial H_1}{\partial x} + \frac{\partial H_2}{\partial y} = 0, \tag{2}$$

$$u\frac{\partial u}{\partial x} + v\frac{\partial u}{\partial y} = u_e\frac{du_e}{dx} - \frac{\mu_e H_e}{4\pi\rho}\frac{dH_e}{dx} + \nu\frac{\partial^2 u}{\partial y^2} + \frac{\mu_e}{4\pi\rho}\left(H_1\frac{\partial H_1}{\partial x} + H_2\frac{\partial H_1}{\partial y}\right), \tag{3}$$

$$u\frac{\partial H_1}{\partial x} + v\frac{\partial H_1}{\partial y} - H_1\frac{\partial u}{\partial x} - H_2\frac{\partial u}{\partial y} = \varsigma_0\frac{\partial^2 H_1}{\partial y^2}, \tag{4}$$

$$u\frac{\partial T}{\partial x} + v\frac{\partial T}{\partial y} = \alpha\frac{\partial^2 T}{\partial y^2} + \frac{Q_0}{\rho c_p}(T - T_\infty). \tag{5}$$

The boundary conditions are:

$$\begin{array}{l} v = 0,\ u = \lambda u_w(x) = \lambda a x,\ \frac{\partial H_1}{\partial y} = 0,\ H_2 = 0,\ T = T_w \text{ at } y = 0, \\ u(x) \to u_e(x) = ax,\ H_1(x) \to H_0 x,\ T \to T_\infty \text{ when } y \to \infty. \end{array} \tag{6}$$

The dimensionless variables are defined as follows:

$$\begin{array}{l} u = axf'(\eta),\ v = -\sqrt{(a\nu)}\,f(\eta),\ H_1 = H_0 x g'(\eta),\ H_2 = \sqrt{\frac{\nu}{a}}\,H_0 g(\eta), \\ \theta(\eta) = \frac{T - T_\infty}{T_w - T_\infty},\ \eta = \sqrt{\frac{a}{\nu}}\,y, \end{array} \tag{7}$$

where primes denote differentials with respect to η. Equations (1) and (2) are identically satisfied. Substituting (7) into Equations (3)–(6) reduces the equations to:

$$f''' + ff'' - f'^2 + 1 + M\left(g'^2 - gg'' - 1\right) = 0, \tag{8}$$

$$\varepsilon g''' + f g'' - f'' g = 0, \tag{9}$$

$$\theta'' + \Pr(f\theta' + Q\theta) = 0. \tag{10}$$

The boundary conditions become:

$$\begin{array}{l} f(0) = 0,\ f'(0) = \lambda,\ g(0) = 0,\ g''(0) = 0,\ \theta(0) = 1, \text{ at } \eta = 0, \\ f'(\eta) \to 1,\ g'(\eta) \to 1,\ \theta(\eta) \to 0 \text{ as } \eta \to \infty \end{array} \tag{11}$$

where $\Pr = \nu/\alpha$ is the Prandtl number, $M = (\mu_e/4\pi\rho)\,(H_0/a)^2$ is the magnetic parameter, $\varepsilon = \varsigma_0/\nu$ is the reciprocal of the magnetic Prandtl number and $Q = Q_0/(a\rho c_p)$ is the heat generation ($Q > 0$) or absorption ($Q < 0$).

We note that when $M = 0$ (without the magnetic field), this problem reduces to that of Mahapatra and Gupta [32]. In fact, when the magnetic field is absent, Equation (9) is no longer necessary [28].

The quantities of physical interest include the skin friction coefficient and the local Nusselt number, which are given as [33]:

$$C_f = \frac{\tau_w}{\rho u_e^2(x)},\ Nu_x = \frac{x q_w}{k(T_w - T_\infty)}, \tag{12}$$

where τ_w is the surface shear stress and q_w is the surface heat flux which, respectively, are given by:

$$\tau_w = \mu\left(\frac{\partial u}{\partial y}\right)_{y=0},\ q_w = -k\left(\frac{\partial T}{\partial y}\right)_{y=0}. \tag{13}$$

Using (7), (12) and (13), one gets:

$$\mathrm{Re}_x{}^{1/2} C_f = f''(0),\ \mathrm{Re}_x{}^{-1/2} Nu_x = -\theta'(0), \tag{14}$$

where $\mathrm{Re}_x = xu_e/\nu$ is the local Reynolds number.

3. Flow Stability

The temporal stability analysis is performed to determine the stability of the solutions in the long run. To do this, we consider the unsteady case for the present problem. The unsteady form of Equations (8)–(10) are given as:

$$\frac{\partial u}{\partial t} + u\,\frac{\partial u}{\partial x} + v\,\frac{\partial u}{\partial y} = u_e \frac{du_e}{dx} - \frac{\mu_e h_e}{4\pi\rho}\,\frac{dH_e}{dx} + \nu\,\frac{\partial^2 u}{\partial y^2} + \frac{\mu_e}{4\pi\rho}\left(H_1 \frac{\partial H_1}{\partial x} + H_2 \frac{\partial H_2}{\partial y}\right), \tag{15}$$

$$\frac{\partial u}{\partial t} + u\,\frac{\partial H_1}{\partial x} + v\,\frac{\partial H_1}{\partial y} - H_1 \frac{\partial u}{\partial x} - H_2 \frac{\partial u}{\partial y} = \varsigma_0 \frac{\partial^2 H_1}{\partial y^2}, \tag{16}$$

$$\frac{\partial T}{\partial t} + u\,\frac{\partial T}{\partial x} + v\,\frac{\partial T}{\partial y} = \alpha\,\frac{\partial^2 T}{\partial y^2} + \frac{Q_0}{\rho c_p}(T - T_\infty). \tag{17}$$

Following the works of Weidman et al. [34], Roşca and Pop [35] and Waini et al. [36], the new time-dependent variables are introduced as:

$$\begin{aligned} &U = aX\tfrac{\partial f}{\partial Y}(\eta,\tau),\ V = -\sqrt{a\nu}\tfrac{\partial f}{\partial Y}(\eta,\tau),\ \theta(\eta,\tau) = \tfrac{T-T_\infty}{T_w-T_\infty},\ H_1 = H_0 X \tfrac{\partial g}{\partial Y}(\eta,\tau),\\ &H_2 = -\sqrt{\tfrac{\nu}{a}}\,H_0 \tfrac{\partial g}{\partial Y}(\eta,\tau),\ \eta = \sqrt{\tfrac{a}{\nu}}\,y, \end{aligned} \tag{18}$$

where $\tau = at$, so that Equations (15)–(17) for the unsteady case may be written as:

$$\frac{\partial^3 f}{\partial Y^3} + f\,\frac{\partial^2 f}{\partial Y^2} - \left(\frac{\partial f}{\partial Y}\right)^2 + 1 + M\left[\left(\frac{\partial g}{\partial Y}\right)^2 - g\,\frac{\partial^2 g}{\partial Y^2} - 1\right] - \frac{\partial^2 f}{\partial \eta \partial \tau} = 0, \tag{19}$$

$$\varepsilon\,\frac{\partial^3 g}{\partial Y^3} + f\,\frac{\partial^2 g}{\partial Y^2} - g\,\frac{\partial^2 f}{\partial Y^2} - \frac{\partial^2 g}{\partial \eta \partial \tau} = 0, \tag{20}$$

$$\frac{\partial^2 h}{\partial Y^2} + \mathrm{Pr}\left(f\,\frac{\partial h}{\partial Y} + Qh\right) - \frac{\partial h}{\partial \tau} = 0, \tag{21}$$

subject to:

$$\begin{aligned} &f(0,\tau) = 0,\ \tfrac{\partial f}{\partial Y}(0,\tau) = \lambda,\ g(0,\tau) = 0,\ \tfrac{\partial^2 g}{\partial Y^2}(0,\tau) = 0,\ h(0,\tau) = 1 \text{ at } Y = 0,\\ &\tfrac{\partial f}{\partial Y}(Y,\tau) \to 1,\ \tfrac{\partial g}{\partial Y}(Y,\tau) \to 1,\ h(Y,\tau) \to 0 \text{ as } Y \to \infty. \end{aligned} \tag{22}$$

To test the stability of the solutions of the system of Equations (8)–(10), the basic solutions $f = f_0(\eta)$, $g = g_0(\eta)$ and $h = h_0(\eta)$ with the disturbances perturbed as [34–37] are:

$$f(\eta,\tau) = f_0(\eta) + e^{-\gamma\tau}F(\eta),\ g(\eta,\tau) = g_0(\eta) + e^{-\gamma\tau}G(\eta),\ h(\eta,\tau) = h_0(\eta) + e^{-\gamma\tau}H(\eta) \tag{23}$$

where γ is an unknown eigenvalue and $F(\eta)$, $G(\eta)$ and $H(\eta)$ are relatively small compared to $f_0(\eta)$, $g_0(\eta)$ and $h_0(\eta)$. Substituting (23) into Equations (19)–(22), and after linearization, the following system is obtained:

$$F''' + f_0 F'' + f_0''\,F + M(2g_0'\,G' - g_0 G'' - g_0''\,G) - (2f_0' - \gamma)F' = 0, \tag{24}$$

$$\varepsilon G''' + f_0 G'' + g_0''\,F - f_0''\,G - g_0 F'' + \gamma G' = 0, \tag{25}$$

$$H'' + \mathrm{Pr}(f_0 H' + h_0'\,F) + (\mathrm{Pr}Q + \gamma)H = 0, \tag{26}$$

$$F(0) = 0,\ F'(0) = 0,\ G(0) = 0,\ G'(0) = 0,\ H = 0,\ \text{at } Y = 0,$$
$$F'(Y) \to 0,\ G'(Y) \to 0,\ H(Y) \to 0 \text{ as } Y \to \infty. \tag{27}$$

Without the loss of generality, the smallest eigenvalues γ in Equations (24)–(27) are obtained by setting $F''(0) = 1$. From Equation (23), if γ is negative, then there is an initial growth of disturbances and thus the flow is unstable, as $\tau \to \infty$. However, when γ is positive, the disturbances vanish as $\tau \to \infty$ and thus the flow is stable.

4. Result and Discussion

The system of Equations (8)–(10) was solved numerically using the boundary value problem solver bvp4c built in MATLAB software (R2019b, The MathWorks, Inc., Natick, MA, USA) for different values of M, ε and Q while the Prandtl number, Pr, is fixed at 1.0 (such as ionized gases). This solver used a third order Lobatto IIIa formula with a collocation method for solving the boundary value problem. The numerical results obtained are compared with those reported by Rosca et al. [38] and Ishak et al. [39] when $M = 0$ for both stretching and shrinking cases. Table 1 shows the comparison of $f''(0)$ with those of Rosca et al. [38] and Ishak et al. [39]. From the table, it is seen that they are in a good agreement, which gives confidence to the numerical results for other values of parameters.

Table 1. Comparison of $f''(0)$ for $M = 0$ and $\lambda < 0$ (shrinking sheet).

λ	Present Study		Ishak et al. [39]		Rosca et al. [38]	
	Upper Branch	Lower Branch	Upper Branch	Lower Branch	Upper Branch	Lower Branch
−0.5	1.495690	-	1.495670	-	1.495669	-
−0.75	1.489298	-	1.489298	-	1.489298	-
−1	1.328817	0.0	1.328817	0.0	1.328816	0.0
−1.15	1.082231	0.116702	1.082231	0.116702	1.082231	0.116702
−1.20	0.932473	0.233650	0.932474	0.233650	0.932473	0.233649

Table 2 shows that for fixed values of Pr, ε, Q and λ, the skin friction coefficient $f''(0)$ and the local Nusselt number $-\theta'(0)$ decrease as the magnetic parameter M increases for the upper branch solution. However, for the lower branch solution, the skin friction coefficient and the local Nusselt number increase as the magnetic parameter increases. As the value of M increases, the local Nusselt number decreases for the lower branch solution only. Moreover, Table 3 shows the variation of the local Nusselt number for various values of the heat generation Q. We note that $Q > 0$ is for the heat generation, while $Q < 0$ is for the heat absorption. It is observed that increasing the heat generation will prompt the local Nusselt number to increase for both upper and lower branch solutions. Based on Fourier's law, the negative temperature gradient across the surface will increase when the heat generation increases.

Table 2. Variation of $\mathrm{Re}^{(1/2)}{}_x C_f$ and $\mathrm{Re}^{(-1/2)}{}_x Nu_x$ with Pr = 1, ε = 1000, Q = 0.1 dan λ= −1.2.

M	$\mathrm{Re}^{(1/2)}{}_x C_f$		$\mathrm{Re}^{(-1/2)}{}_x Nu_x$	
	Upper Branch	Lower Branch	Upper Branch	Lower Branch
0.1	0.919288600	0.245461561	0.036388462	0.135535051
0.5	0.860316623	0.299225512	0.049914145	0.135168459
1.0	0.761569269	0.392040873	0.071787829	0.130550670

Table 3. Variation of $\mathrm{Re}^{(-1/2)}{}_x \mathrm{Nu}_x$ with Pr = 1.0, M = 0.1, ε = 1000 and λ = −1.2.

	Q	0	0.2	0.5
$\mathrm{Re}^{(-1/2)}{}_x Nu_x$	Upper branch solution	−0.093149185	0.194299118	1.160454023
	Lower branch solution	−0.002856956	0.304206653	1.362866119

Figure 2 demonstrates the variation of the skin friction coefficient with $\lambda < 0$ for the magnetic parameter $M = 0, 0.5, 1.0$ where $\varepsilon = 1000$, $Q = 0.1$ (heat generation) and Pr = 1.0 (such as ionized gases). It is observed that increasing the magnetic parameter M will decrease the range of λ for which the solutions are in existence. There exist two solutions, upper and lower branch solutions, for $\lambda < 0$ (shrinking case). The magnetic parameter gives influence to the skin friction coefficient, as can be seen in Figure 2, the skin friction coefficient decreases when M increases, for all values of λ presented in this figure.

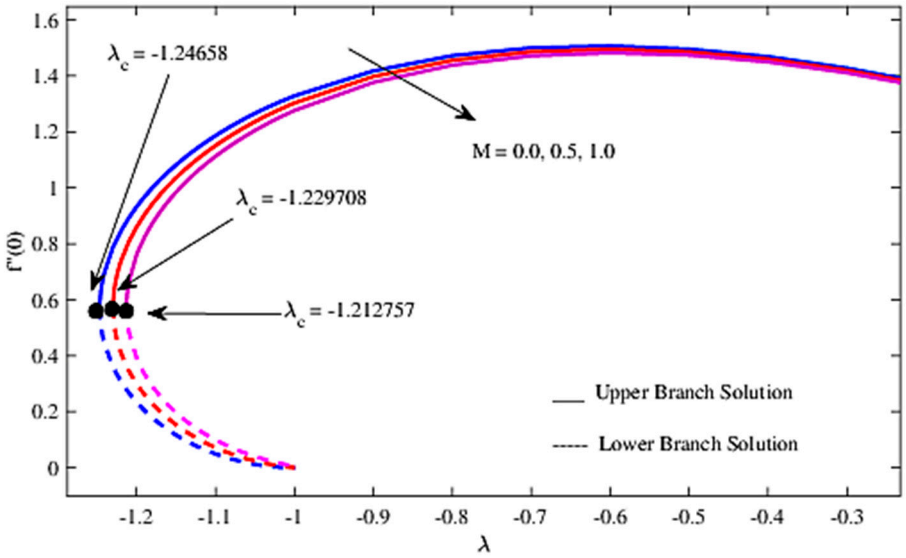

Figure 2. Variation of the skin friction coefficient $f''(0)$ with λ for different values of M with $\varepsilon = 1000$, $Q = 0.1$ and Pr = 1.0.

The variation of the local Nusselt number $-\theta'(0)$ with $\lambda < 0$ for $M = 0, 0.5, 1.0$ with Pr = 1.0, $\varepsilon = 1000$ and $Q = 0.1$ (heat generation) is shown in Figure 3. It also discovers that the magnitude of the critical value λ_c slightly decreases as M increases. The magnetic parameter M also influences the local Nusselt number to decrease as the values of M increases.

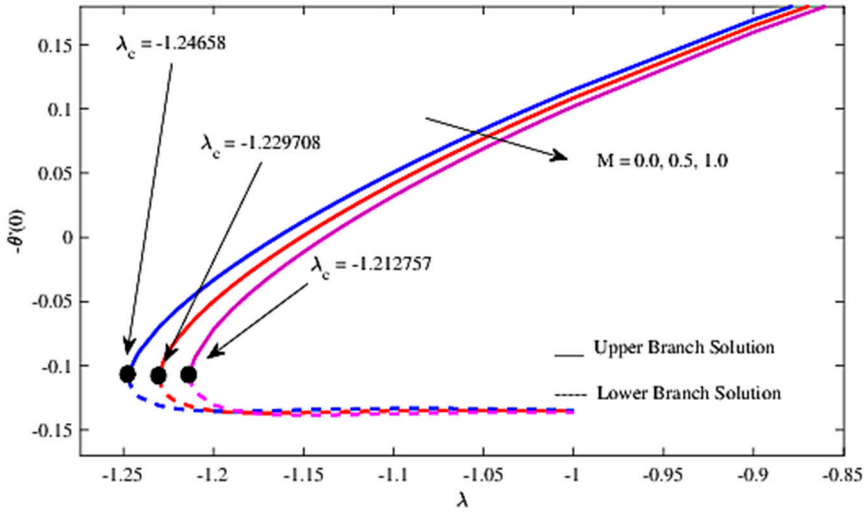

Figure 3. Variation of the Nusselt number $-\theta'(0)$ with λ for different values of M with $\varepsilon = 1000$, $Q = 0.1$ and Pr = 1.0.

The velocity and temperature profiles for several values of M, ε and Q are shown in Figures 4–8, respectively. From Figure 4, the velocity decreases as M increases for the upper branch solution and on

the contrary, the velocity increases for the lower branch solution. This is due to the increase in the magnetic field that will cause a reduction in the velocity of the fluid as the magnetic field is inversely proportional to the velocity of the fluid. It can be observed that the reciprocal of the magnetic Prandtl number ε can influence the velocity of the fluid which is shown in Figure 5. The velocity $f'(\eta)$ increases as the value of ε increases for the upper branch solution, but for the lower branch solution, the velocity decreases. These results occur because the electrical conductivity decreases as ε increases. Hence, the velocity in the boundary layer will lose control of the magnetic lines of forces. This phenomenon has been explained by Takhar et al. [40].

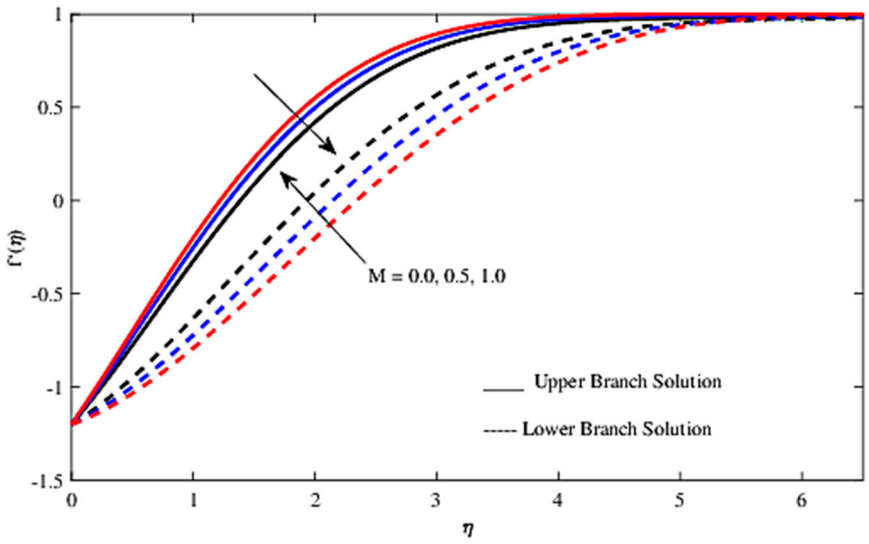

Figure 4. Velocity profiles $f'(\eta)$ for several values of M when λ = −1.2, ε = 1000, Q = 0.1 and Pr = 1.0.

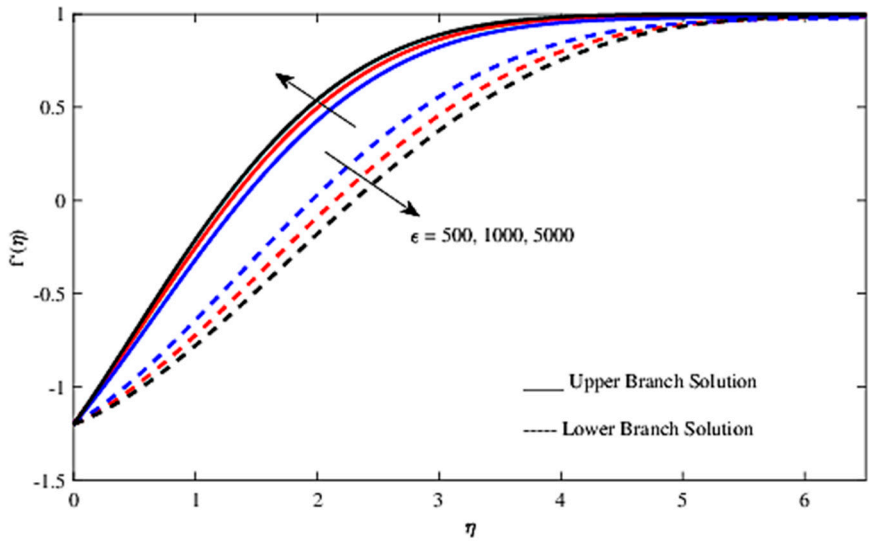

Figure 5. Velocity profiles $f'(\eta)$ for several values of ε when λ = −1.2, M = 0.5, Q = 0.1 and Pr = 1.0.

It is worth observing the temperature of the fluid in the absence of M, and also when M is acting on the surface which is presented in Figure 6. It can be observed that when M increases, the temperature of the fluid increases for the upper branch solution but the temperature decreases for the lower branch solution. This phenomenon happens as an increase in the magnetic field will enhance the generation of heat. Hence, the temperature of the fluid will be forced to increase. This is in accordance with the results published in the previous work [41].

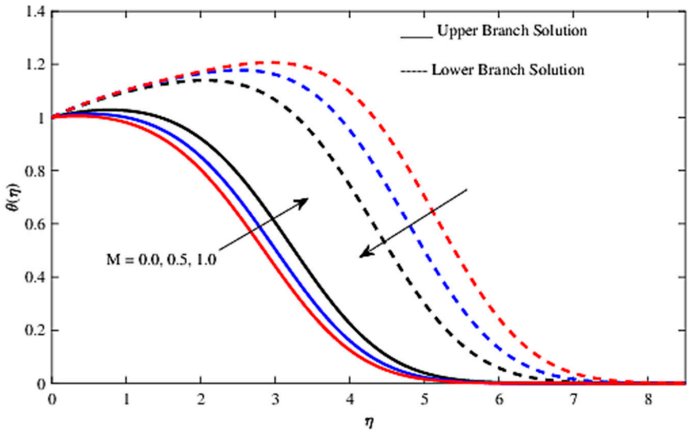

Figure 6. Temperature profiles $\theta(\eta)$ for several values of M when $\lambda = -1.2$, $\varepsilon = 1000$, $Q = 0.1$ and $\mathrm{Pr} = 1.0$.

Furthermore, Figure 7 shows the temperature profiles for several values of ε which indicates that the temperature is decreasing by increasing the values of ε. However, it is only true for the upper branch solution. As for the lower branch solution, the temperature increases as ε increases. Figure 8 presents the dimensionless temperature profiles with the influence of Q. It reveals that the parameter Q increases the temperature of the fluid for both upper and lower branch solutions. This is explained by Fourier's law mentioned above.

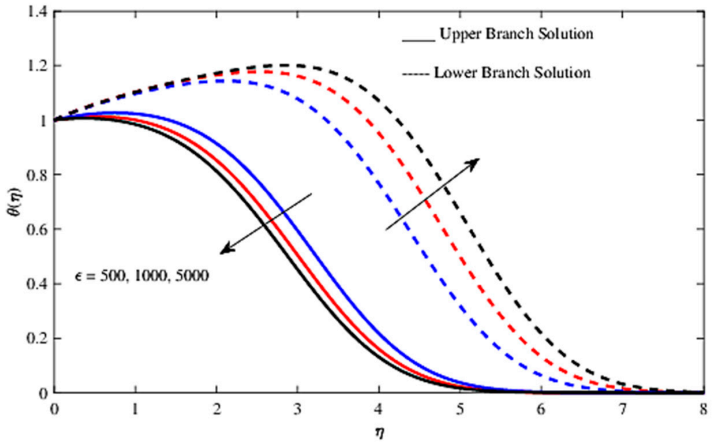

Figure 7. Temperature profiles $\theta(\eta)$ for several values of ε when $\lambda = -1.2$, $\mathrm{M} = 0.5$, $\mathrm{Q} = 0.1$ and $\mathrm{Pr} = 1.0$.

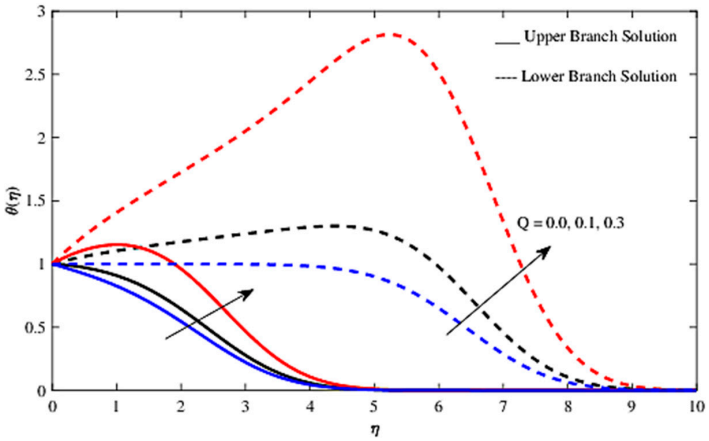

Figure 8. Temperature profiles $\theta(\eta)$ for several values of Q when $\lambda = -1.2$, $\varepsilon = 1000$, $M = 0.5$ and $\mathrm{Pr} = 1.0$.

In this paper, dual solutions are obtained when $\lambda < 0$ (shrinking case). The temporal stability is analyzed to determine which solution is stable as time evolves, by finding the eigenvalues γ in the system of Equations (24)–(27). Due to the relations in Equation (23), negative values of γ produce a disturbance as $\tau \to \infty$, and thus the flow becomes unstable. On the other hand, positive values of γ result in diminished disturbance, thus the flow is stable in the long run. Figure 9 shows the values of γ for selected values of λ. It is noticeable from this figure that γ is positive for the first solution (upper branch), but negative for the second solution (lower branch). Thus, the first solution is stable, but the second solution is unstable, see also [42].

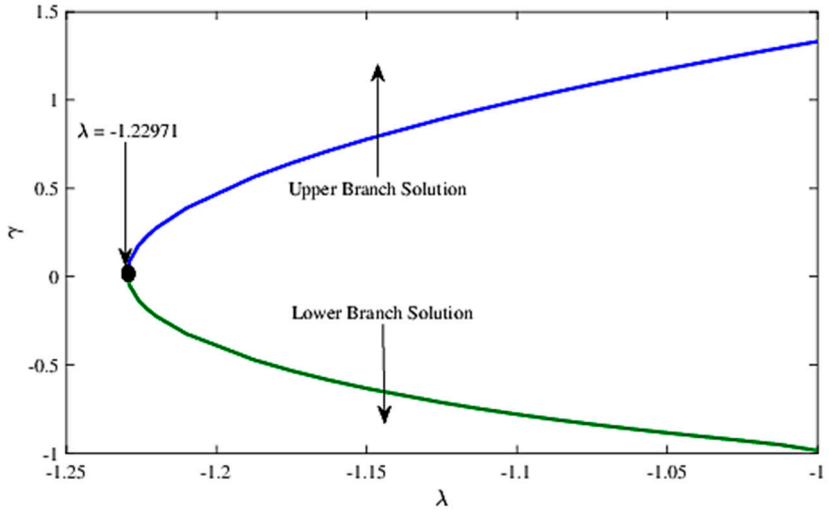

Figure 9. The smallest eigenvalues γ for selected values of λ.

5. Conclusions

This study investigated the MHD flow induced by a shrinking/stretching sheet where the induced magnetic field is taken into consideration. The numerical results obtained showed that both the skin friction coefficient and the local Nusselt number decreased with increasing values of the magnetic parameter M. The magnetic parameter M enhanced the temperature but reduced the velocity inside the boundary layer. Moreover, increasing the reciprocal of the magnetic Prandtl number ε caused an increase in the velocity but a decrease in the temperature inside the boundary layer. The presence of the heat source $Q > 0$ greatly affected the temperature of the fluid. Two solutions were found for a single value of the parameter. The first and the second solutions are separated at the eigenvalue $\gamma = 0$. The smallest value for which the solutions are in existence is $\lambda = -1.22971$. The solution is not possible for large and moderately shrinking strength. The temporal stability analysis revealed that the first solution is stable in the long run while the second solution is unstable.

Author Contributions: Conceptualization, I.P.; funding acquisition, A.I.; methodology, N.A.A.M.N.; project administration, A.I.; supervision, A.I. and I.P.; validation, I.P.; writing—original draft, N.A.A.M.N.; writing—review and editing, A.I., I.P. All authors have read and agreed to the published version of the manuscript.

Funding: This work was supported by a research grant from the Ministry of Education, Malaysia. The grant number is FRGS/1/2019/STG06/UKM/01/4.

Acknowledgments: The authors wish to express their very sincere thanks to the anonymous reviewers for their valuable comments and suggestions. This work was supported by a research grant (Project Code: FRGS/1/2019/STG06/UKM/01/4) from the Ministry of Education, Malaysia.

Conflicts of Interest: The authors declare no conflict of interest.

Nomenclatures

C_f	Skin friction coefficient
c_p	Specific heat at constant pressure (JKg^{-1} K^{-1})
ρc_p	Heat capacitance of the fluid (JK^{-1} m^{-3})
$f(\eta)$	Dimensionless stream function
H_0	Initial velocity magnetic field
H_1, H_2	Velocity magnetic field component in x and y direction
H_e	Velocity magnetic field of the ambient fluid
Nu_x	Local Nusselt number
Pr	Prandtl number
Q_0	Thermal conductivity
Re_x	Local Reynolds number
T	Fluid temperature (K)
T_w	Surface temperature (K)
T_∞	Ambient temperature (K)
T	Time (s)
U, V	Velocity component time dependent in the x and y directions (ms^{-1})
u, v	Velocity components in the x and y directions (ms^{-1})
u_w	Velocity of the surface (ms^{-1})
u_e	Ambient velocity (ms^{-1})
Greek symbols	
α	Thermal diffusivity
γ	Eigenvalue
ζ_0	Magnetic diffusivity
η	Similarity variable
λ	Shrinking parameter
θ	Dimensionless temperature
μ	Dynamic viscosity of the fluid (kgm^{-1}s^{-1})
ν	Kinematic viscosity of the fluid (m^2 s^{-1})
ρ	Density of the fluid (kgm^{-3})
τ_w	Skin friction or wall shear stress (kgm^{-1}s^{-2})
τ	Dimensionless time
Subscripts	
f	Fluid
Superscript	
$'$	Differentiation with respect to η

References

1. Rashad, A.M. Impact of thermal radiation on MHD slip flow of a ferrofluid over a non-isothermal wedge. *J. Magn. Magn. Mater.* **2017**, *422*, 25–31. [CrossRef]
2. Hassan, M.; Marin, M.; Alsharif, A.; Ellahi, R. Convection heat transfer flow of nanofluid in a porous medium over wavy surface. *Phys. Lett. A* **2018**, *382*, 2749–2753. [CrossRef]
3. Jha, B.K.; Aina, B. Role of induced magnetic field on MHD natural convection flow in vertical microchannel formed by two electrically non-conducting infinite vertical parallel plates. *Alex. Eng. J.* **2016**, *55*, 2087–2097. [CrossRef]
4. Fang, T. Magnetohydrodynamic viscous flow over a nonlinearly moving surface: Closed-form solutions. *Eur. Phys. J. Plus* **2014**, *129*, 92. [CrossRef]
5. Goldsworthy, F.A. Magnetohydrodynamic flow of a perfectly conducting, viscous fluid. *J. Fluid Mech.* **1961**, *11*, 519–528. [CrossRef]
6. Zhang, J.; Fang, T.; Zhong, Y.F. Analytical solution of magnetohydrodynamic sink flow. *Appl. Math. Mech. Engl.* **2011**, *32*, 1221–1230. [CrossRef]

7. Alamri, S.Z.; Khan, A.A.; Azeez, M.; Ellahi, R. Effects of mass transfer on MHD second grade fluid towards stretching cylinder: A novel perspective of Cattaneo-Christov heat flux model. *Phys. Lett. A* **2019**, *383*, 276–281. [CrossRef]
8. Yousif, M.A.; Ismael, H.K.; Abbas, T.; Ellahi, R. Numerical study of momentum and heat transfer of MHD Carreaunanofluid over an exponentially stretched plate with internal heat source/sink and radiation. *Heat Transf. Res.* **2019**, *50*, 649–658. [CrossRef]
9. Fang, T.; Zhang, J.; Yao, S. Slip MHD viscous flow over a stretching sheet—An exact solution. *Commun. Nonlinear Sci. Numer. Simul.* **2009**, *14*, 3731–3737. [CrossRef]
10. Fang, T.; Zhang, J. Closed-form exact solutions of MHD viscous flow over a shrinking sheet. *Commun. Nonlinear Sci. Numer. Simul.* **2009**, *14*, 2853–2857. [CrossRef]
11. Nandy, S.K.; Sidui, S.; Mahapatra, T.R. Unsteady MHD boundary-layer flow and heat transfer of nanofluid over a permeable shrinking sheet in the presence of thermal radiation. *Alex. Eng. J.* **2014**, *53*, 929–937. [CrossRef]
12. Akbar, N.S.; Nadeem, S.; Ul-Haq, R.; Yex, S. MHD stagnation point flow of Carreau fluid toward a permeable shrinking sheet: Dual solutions. *Ain Shams Eng. J.* **2014**, *5*, 1233–1239. [CrossRef]
13. Ghosh, S.; Mukhopadhyay, S.; Vajravelu, K. Dual solutions of slip flow past a nonlinearly shrinking permeable sheet. *Alex. Eng. J.* **2016**, *55*, 1835–1840. [CrossRef]
14. Nadeem, S.; Ul-Haq, R.; Lee, C. MHD flow of a Casson fluid over an exponentially shrinking sheet. *Sci. Iran.* **2012**, *19*, 1550–1553. [CrossRef]
15. Rosali, H.; Ishak, A.; Nazar, R.; Pop, I. Rotating flow over an exponentially shrinking sheet with suction. *J. Mol. Liq.* **2015**, *211*, 965–969. [CrossRef]
16. Rosca, N.C.; Rosca, A.V.; Pop, I. Lie group symmetry method for MHD double-diffusive convection from a permeable vertical stretching/shrinking sheet. *Comput. Math. Appl.* **2016**, *71*, 1679–1693. [CrossRef]
17. Turkyilmazoglu, M. MHD fluid flow and heat transfer due to a shrinking rotating disk. *Comput. Fluids* **2014**, *90*, 51–56. [CrossRef]
18. Soid, S.K.; Ishak, A.; Pop, I. Unsteady MHD flow and heat transfer over a shrinking sheet with ohmic heating. *Chin. J. Phys.* **2017**, *55*, 1626–1636. [CrossRef]
19. Fang, T.; Wang, F. Viscous slip MHD flow over a moving sheet with an arbitrary surface velocity. *Chin. Phys. Lett.* **2018**, *35*, 104701. [CrossRef]
20. Hiemenz, K. Die grenzschicht an einem in den gleichformingen flussigkeitsstrom eingetauchten geraden kreiszylinder. *Dinglers Polytech. J.* **1911**, *326*, 321–324.
21. Mustafa, I.; Javed, T.; Ghaffari, A. Heat transfer in MHD stagnation point flow of a ferrofluid over a stretchable rotating disk. *J. Mol. Liq.* **2016**, *219*, 526–532. [CrossRef]
22. Ibrahim, W. The effect of induced magnetic field and convective boundary condition on MHD stagnation point flow and heat transfer of upper-convected Maxwell fluid in the presence of nanoparticle past a stretching sheet. *Propuls. Power Res.* **2016**, *5*, 164–175. [CrossRef]
23. Mabood, F.; Khan, W.A.; Ismail, A.M. MHD stagnation point flow and heat transfer impinging on stretching sheet with chemical reaction and transpiration. *Chem. Eng. J.* **2015**, *273*, 430–437. [CrossRef]
24. Farooq, M.; Khan, M.I.; Waqas, M.; Hayat, T.; Alsaedi, A.; Khan, M.I. MHD stagnation point flow of viscoelastic nanofluid with non-linear radiation effects. *J. Mol. Liq.* **2016**, *221*, 1097–1103. [CrossRef]
25. Rostami, M.N.; Dinarvand, S.; Pop, I. Dual solutions for mixed convective stagnation-point flow of an aqueous silica-alumina hybrid nanofluid. *Chin. J. Phys.* **2018**, *56*, 2465–2478. [CrossRef]
26. Nasir, N.A.A.M.; Ishak, A.; Pop, I. Stagnation-point flow and heat transfer past a permeable quadratically stretching/shrinking sheet. *Chin. J. Phys.* **2017**, *55*, 2081–2091. [CrossRef]
27. Khan, M.I.; Kiyani, M.Z.; Malik, M.Y.; Yasameen, T.; Khan, M.W.A.; Abbas, T. Numerical investigation of magnetohydrodynamic stagnation point flow with variable properties. *Alex. Eng. J.* **2016**, *55*, 2367–2373. [CrossRef]
28. Ali, F.M.; Nazar, R.; Arifin, N.M.; Pop, I. MHD boundary layer flow and heat transfer over a stretching sheet with induced magnetic field. *Heat Mass Transf.* **2011**, *47*, 155–162. [CrossRef]
29. Ali, F.M.; Nazar, R.; Arifin, N.M.; Pop, I. MHD stagnation-point flow and heat transfer towards stretching sheet with induced magnetic field. *Appl. Math. Mech. Engl.* **2011**, *32*, 409–418. [CrossRef]
30. Goldstein, S. On backward boundary layers and flow in converging passage. *J. Fluid Mech.* **1965**, *21*, 33–45. [CrossRef]

31. Cowling, T.G. *Magnetohydrodynamics*; Interscience Publishers: New York, NY, USA; London, UK, 1957.
32. Mahapatra, T.R.; Gupta, A.S. Heat transfer in stagnation-point flow towards a stretching sheet. *Heat Mass Transf.* **2002**, *38*, 517–521. [CrossRef]
33. Zeeshan, A.; Shehzad, N.; Abbas, T.; Ellahi, R. Effects of radiative electro-Magnetohydrodynamics diminishing internal energy of pressure-driven flow of titanium dioxide-water nanofluid due to entropy generation. *Entropy* **2019**, *21*, 236. [CrossRef]
34. Weidman, P.D.; Kubitschek, D.G.; Davis, A.M.J. The effect of transpiration on self similar boundary layer flow over moving surfaces. *Int. J. Eng. Sci.* **2006**, *44*, 730–737. [CrossRef]
35. Rosca, N.C.; Pop, I. Mixed convection stagnation point flow past a vertical flat plate with a second order slip: Heat flux case. *Int. J. Heat Mass Transf.* **2013**, *65*, 102–109. [CrossRef]
36. Waini, I.; Ishak, A.; Pop, I. Squeezed hybrid nanofluid flow over a permeable sensor surface. *Mathematics* **2020**, *8*, 898. [CrossRef]
37. Harris, S.D.; Ingham, D.B.; Pop, I. Mixed convection boundary-layer flow near the stagnation point on a vertical surface in a porous medium: Brinkman model with slip. *Transp. Porous Media* **2009**, *77*, 267–285. [CrossRef]
38. Rosca, A.V.; Rosca, N.C.; Pop, I. Numerical simulation of the stagnation point flow past a permeable stretching/shrinking sheet with convective boundary condition and heat generation. *Int. J. Numer. Methods Heat* **2016**, *26*, 348–364. [CrossRef]
39. Ishak, A.; Lok, Y.Y.; Pop, I. Stagnation-point flow over a shrinking sheet in a micropolar fluid. *Chem. Eng. Commun.* **2010**, *197*, 1417–1427. [CrossRef]
40. Takhar, H.S.; Chamkha, A.J.; Nath, G. Unsteady flow and heat transfer on a semi-infinite at plate with an aligned magnetic. *Int. J. Eng. Sci.* **1999**, *37*, 1723–1736. [CrossRef]
41. Sarafraz, M.M.; Pourmehran, O.; Yang, B.; Arjomandi, M.; Ellahi, R. Pool boiling heat transfer characteristics of iron oxide nano-suspension under constant magnetic field. *Int. J. Therm. Sci.* **2020**, *147*, 106131. [CrossRef]
42. Dhanai, R.; Rana, P.; Kumar, L. MHD mixed convection nanofluid flow and heat transfer over an inclined cylinder due to velocity and thermal slip effects: Buongiorno's model. *Powder Technol.* **2016**, *288*, 140–150. [CrossRef]